Microstructural and mechanical effects of nickel and manganese on high strength steel weld metals

E. Keehan, H. O. Andrén

Chalmers University of Technology, Gothenburg, Sweden.

L. Karlsson

ESAB AB, Gothenburg, Sweden

M. Murugananth, H. K. D. H. Bhadeshia
University of Cambridge, United Kingdom.

Abstract

Neural network modelling suggested that the impact strength of high-strength steel weld metals could be increased at moderate expense to yield strength once Ni additions are made in a controlled manner with respect to Mn. Based on these predictions, shielded metal arc welding was used to prepare weld metals with Ni at 7 and 9 wt. % while Mn was at 2.0 or 0.5 wt. %. Tensile testing showed that these new weld metals have yield strengths between 720 and 850 MPa. Charpy toughness levels up to 113 J at -40 °C were recorded. It was found that once Ni exceeds a critical point, which depends on Mn concentration, toughness decreases. LOM, SEM, TEM and APFIM was used to characterize the microstructure that consisted of retained austenite, martensite and bainite. EDX and SIMS showed segregation of Mn and Ni to dendrite boundary regions. APFIM brought greater understanding of the microstructural composition at a local level. Correlations were made between the microstructure and mechanical properties.

Introduction

The aim of increasing toughness at low temperatures while still maintaining yield strength greater than 690 MPa in high-strength steel weld metals has been a constant topic of research in the last two decades. In many applications it is a requirement that over-matching weld metals are used in order to avoid design limitations. Toughness is possible to achieve with welding methods such as gas-tungsten arc welding (GTAW) under well controlled conditions, but becomes more problematic with more flexible and productive methods such as shielded metal arc welding (SMAW), flux cored arc welding (FCAW), or submerged arc welding (SAW) [1, 2].

To date many have carried out research by varying elemental composition and weld parameters with the hope of achieving good toughness using SMAW. Lord, successfully increased toughness to 74 J at - 60 °C with Ni additions from 3 to 4 wt. % at decreasing Mn levels from 1.1 to 0.8 wt. %. A yield strength of 809 MPa was reported for this weld alloy

[3]. Kang followed this trend of increasing Ni and reducing Mn. The best toughness achieved (55 J at - 60 °C) was with Ni at 6.95 wt. % and Mn at 0.52 wt. %. A predicted yield strength of 684 MPa was reported from hardness measurements of this alloy [4].

Recently new development routes have been introduced to material science with neural network modelling. This technique and the advantages it offers materials science are further described in [5-7]. A neural network model was created with the task of increasing toughness at low temperatures. The model and its parameters are described fully in [8] and only the main results will be presented here. Figure 1 shows contour simulations predicted by artificial neural network models for toughness behaviour at - 40 °C as a function of Mn and Ni concentrations. The model predicted the impact toughness could be increased significantly while still maintaining strength by reducing the Mn concentrations for Ni levels above 5 wt. %. Based on these predictions, it was decided to investigate changes in mechanical and microstructural behaviour in detail for Mn concentrations of 0.5 and 2.0 wt. % with Ni at 7 wt. %. The effect of Ni additions from 7 to 9 wt. % at Mn level at 2.0 wt. % was also chosen for investigation.
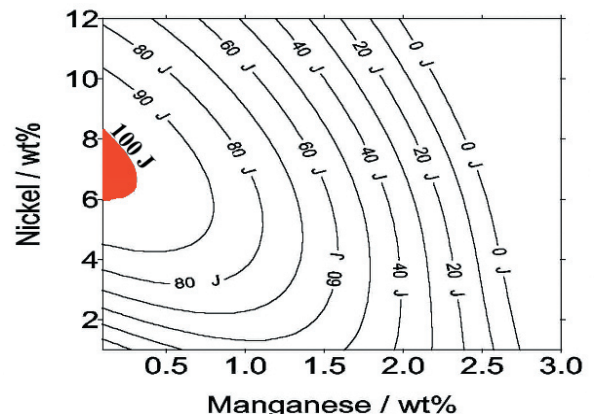

Figure 1. Contour plot showing the predicted behaviour of weld toughness at -40 °C as a function of Mn and Ni concentration.

Experimental Details

Three weld metals were produced using SMAW with Ni at levels of 6.6, 7.2 and 9.2 wt. % while Mn was at 0.6, 2.0 and 2.1 wt. %, respectively. All-weld metals were deposited in accordance with ISO 2560 using buttered 20 mm plates and backing plate. This specific joint geometry allows isolation and accurate characterisation of the weld metal properties. Welding took place in 33 cm runs, with 3 runs per layer and between 22 and 24 beads per joint. Further welding parameters are given in Table 1.

Samples of weld metal were chemically analysed using optical emission spectrometry and Leco combustion equipment. The acquired results are presented in the Table 1.

Charpy impact and tensile testing were performed in compliance with standard EN 10045-1. For Charpy testing, transverse specimens were machined having a cross section of 10×10 mm. These were then notched perpendicular to the welding direction in the weld metal centre and 2 or 3 specimens were tested at each temperature. Tensile specimens were machined longitudinally from the weld deposits with a specimen diameter of 10 mm and a gauge length of 70 mm. Hardness testing was also conducted according to Vickers method using a 10 kg load. Samples were analysed starting in the last bead and then proceeding vertically down the weld metal cross section in 1 mm steps. In total 16 indentations were made on each weld metal.

Specimens from the weld metal cross section, perpendicular to the welding direction were mounted in bakelite for analysis with light optical microscopy (LOM), scanning electron microscopy (SEM) and secondary ion mass spectroscopy (SIMS). These were wet ground and polished to 1 μm diamond grain size. Prior to LOM the microstructure was exposed using 2 % nital etchant. SEM investigations took place on both polished samples (to allow back scattered imaging and energy dispersive X-ray analysis (EDX)) and etched specimens (allowing mircrostructural characterisation). For TEM studies, 3 mm disc shape specimens perpendicular to the welding direction were ground to between 50 and 80 μm in thickness. The discs were then jet electropolished using 10 % perchloric acid in methanol at -35 °C.

Atom probe field ion microscopy (APFIM) was performed on the last bead of weld alloys 1 and 3. Atom probe specimens were prepared by first removing a block of weld metal that included the last bead with approximate dimensions $10 \times 10 \times 15$ mm. The block was subjected to electric discharge machining (EDM) parallel to the welding direction in order to produce rods with approximate dimensions, $0.4 \times 0.4 \times 10$ mm. Rods were then individually removed and electropolished to produce needle shape specimens with a tip radius of less that 50 nm using standard electropolishing methods [9]. The APFIM instrument and evaluation system used in these investigations are described elsewhere [10-12]. Atom probe investigations were carried out at specimen temperatures between 55 and 75 K. The residual gas pressure within the UHV chamber was kept below 7×10^{-8} Pa and an evaporation pulse amplitude of 20 % of the standing voltage was applied.

Results

Mechanical Properties. The results from Charpy experiments are presented in Figure 2. A very large variation in toughness is experienced between the first two weld alloys and Alloy 3 which is in a different

Weld Metal	Alloy 1	Alloy 2	Alloy 3
E / kJ mm^{-1}	1.2	1.2	1.0
$T_{I.P.}$ / °C	250	250	250
$\Delta t_{8/5}$ / s	12	11	10
C *	0.032	0.031	0.024
Si	0.25	0.27	0.35
Mn	2.0	2.1	0.6
P	0.011	0.011	0.012
S*	0.008	0.008	0.008
Cr	0.47	0.48	0.21
Ni	7.2	9.2	6.6
Mo	0.63	0.64	0.40
O (ppm)*	380	340	400
N (ppm)*	250	260	197

Table 1. Welding parameters and chemical composition. Welding parameters presented are energy input (E), interpass temperature ($T_{I.P.}$) and the estimated cooling time between 800 and 500 °C ($\Delta t_{8/5}$). Composition is in wt. % unless otherwise stated and '*' indicate elements analysed using Leco combustion equipment.

range. The toughness of Alloy 1 (7.2 Ni, 2.0 Mn) and Alloy 2 (9.2 Ni, 2.1 Mn) is rather poor, reaching 45 J and 16 J, respectively, at room temperature. It is shown that an actual decrease in toughness was experienced as a result of Ni additions with these Mn levels. When the tensile properties (Table 2) are analysed, the yield strengths recorded for both these weld metals were 795 and 848 MPa, respectively. UTS was also high with both achieving over 1000 MPa. Here Ni additions increased strength. As a result of the large difference between YS and UTS the ratio of YS / UTS is well below the commonly required maximum values of 0.85 or 0.9. Elongation is also limited for these alloys.

Looking at Alloy 3 (6.6 Ni, 0.6 Mn) a dramatic increase of toughness is experienced with new levels reached, 101 J at -60 °C. The increase in toughness follows the predictions of the neural network shown in Figure 1. The results verify the model and prove it correct in its estimates that reducing Mn leads to an increase in toughness at the given Ni levels. Looking at Table 2, Alloy 3 has a lower yield strength at 721 MPa, a decrease of 74 MPa from Alloy 1. UTS also decreased to 823 MPa with the decrease in Mn whereas elongation increased to 21 %.

Hardness results for all three alloys are presented in Figure 3. The first seven to eight indents come from the last bead deposited and the
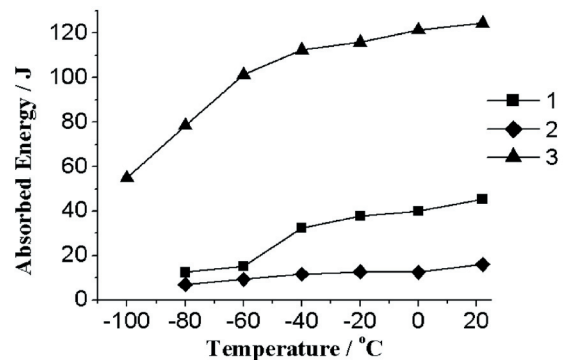

Figure 2. The mean Charpy impact toughness recorded at each temperature for weld Alloys 1-3.

Weld Metal	Alloy 1	Alloy 2	Alloy 3
YS / MPa	795	848	721
UTS / MPa	1006	1051	823
YS / UTS	0.79	0.81	0.88
Elong. / %	15	13	21

Table 2. Tensile properties for the exact compositions and welding parameters of Alloys 1 - 3.
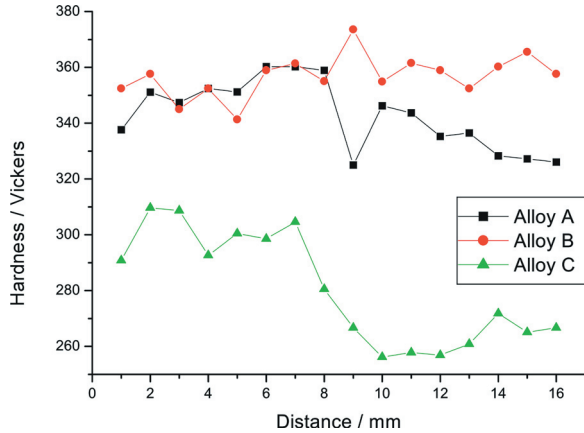

Figure 3. Hardness measurements recorded using Vickers method with a 10 kg load (HV10). Measurements are taken starting at the top of the last bead and proceeding vertically down to the weld metal centre.

Figure 4. LOM micrograph from the last bead of Alloy 3 showing the dendrite boundaries.

remaining come from reheated beads underneath. In the figure it is shown that Alloys 1 and 2 have a much higher hardness than Alloy 3. Also their hardness maintains similar levels with depth in comparison to Alloy 3 where reheated beads are softer than the last bead.

Microstructure. Examination with LOM showed the microstructure in all three alloys has the typical morpology of martensite or bainite with some microslag inclusions which is a characteristic of SMAW weld metals. Figure 4 shows a LOM micrograph taken from the last bead of Alloy 3. Within the micrograph the weld metal dendrites that formed during weld metal solidification are clearly seen.

Analysis of the last bead with SEM in the back scattered mode again showed a clear contrast between the dendrite boundaries and dendrite centres. EDX line scans were carried out across the dendrites and the results are plotted in Figure 5. The plots follow a wave-like pattern with segregation of Mn and Ni to the inter-dendritic regions. In Alloys 1 and
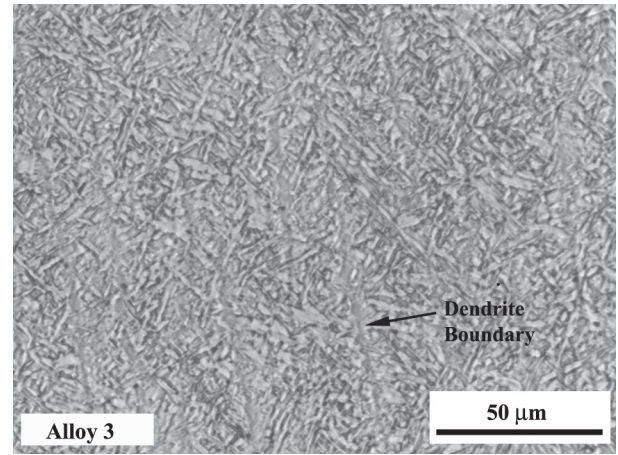
2, Mn and Ni are in phase with each other, both reaching maximum concentrations at the boundaries. Similarly Ni also follows a wave-like pattern in Alloy 3 although Mn segregation is not seen as clearly. To quantify the degree of segregation spot analysis were carried out both at dendrite centres and in inter-dendritic regions. The results presented in Table 3 are the maximum and minimum values recorded. Despite the over quantification of Mn, the results allow a clear comparison and estimate in the degree of segregation between the dendrite boundaries and centres. The greatest difference recorded for both elements between inter-dendritic regions and dendrite centre was 1.15 wt. % for Mn and 2.6 wt. % for Ni in Alloy 2. Alloy 3, with the lowest nominal compositions (0.6 Mn and 6.6 Ni), recorded a difference of 0.38 wt. % and 1.72 wt. % for Mn and Ni, respectively. Since segregation effects seen and recorded with EDX are in one dimension, it was decided to engage SIMS to allow the examination of elemental segregation over a given area to be mapped.

The last bead of all three alloys was again analysed with SIMS and the results are presented in Figure 6. Micrographs are shown for both Mn and Ni and are on a similar scale to LOM micrographs. Each micrograph shows where the individual element is concentrated by appearing brighter in contrast. In all three alloys Mn is segregated to Mn rich inclusions and to inter-dendritic regions. These conclusions were drawn by comparing SIMS micrographs with those from LOM, e.g. comparing results for Alloy 3 in Figure 4 with Figure 6. Along with Mn, Ni segregation to the
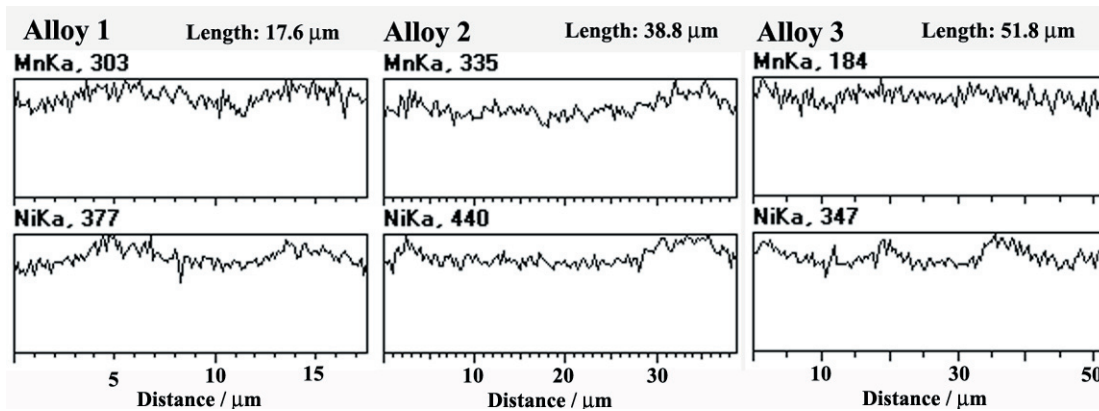

Figure 5. EDX line scans across dendrites in the last bead of Alloys 1 to 3 showing segregation of Ni and Mn.

Weld Metal	Mn	Ni
Alloy 1 Boun	3.1	8.18
Alloy 1 Cent	2.35	6.3
Alloy 2 Boun	3.2	10.3
Alloy 2 Cent	2.05	7.7
Alloy 3 Boun	0.95	7.55
Alloy 3 Cent	0.57	5.83

Table 3. Maximum and minimum compositions recorded in wt. % at dendritic boundary regions (Boun) and dendrite centres (Cent) in the last bead using EDX spot analysis.
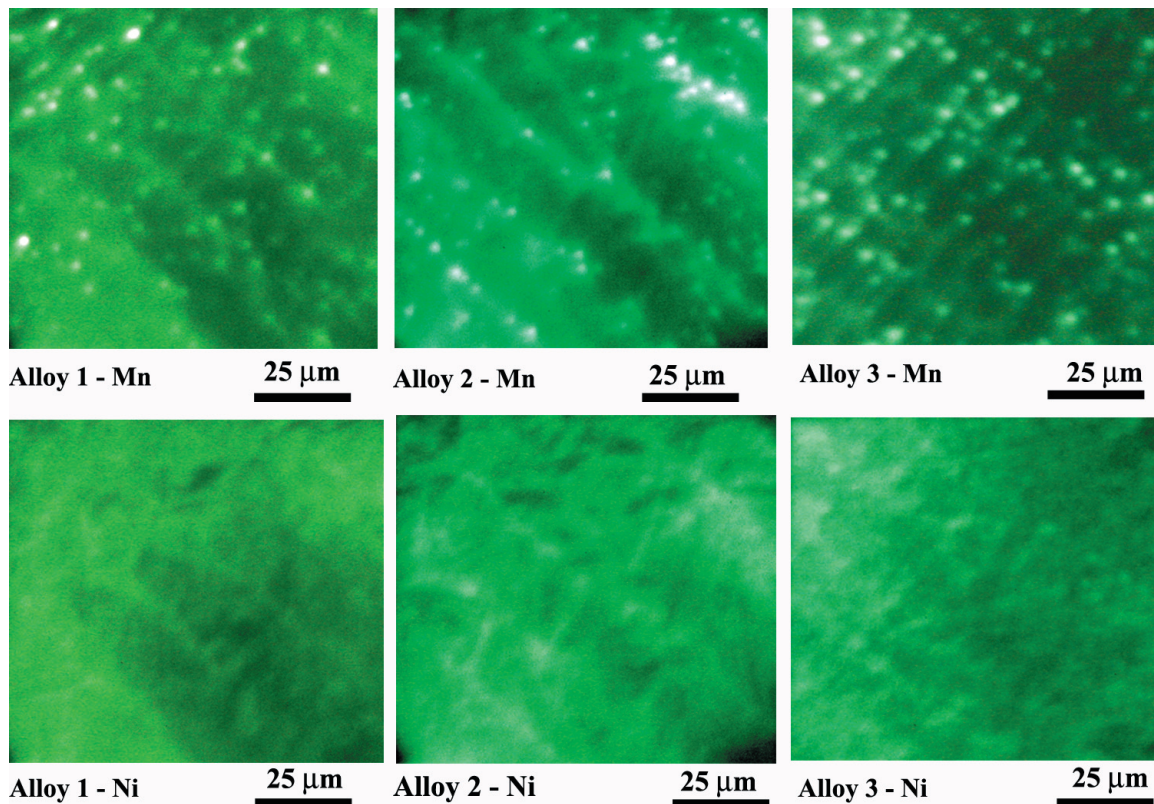
Figure 6. SIMS micrographs showing segregation of Ni and Mn to dendrite boundaries in the last bead of Alloys 1 to 3. Areas where the given element is concentrated appears brighter in contrast. Imaging was carried out using O_2^+ ions.

dendrite boundary regions is seen in all alloys. The greatest segregation effects seen with SIMS was in Alloy 2 which is compatible with results from EDX.

When etched samples were examined with SEM in the secondary electron mode it was concluded the microstructures of all three alloys had the typical morphology of martensite / bainite and the grain morphology changed from coarser to finer grains as Ni increased [13].

TEM investigations were carried out of the last beads of Alloys 1 and 3. It was found the microstructures consisted of martensite, bainite, and retained austenite. Figure 7 shows a bright field image from the last bead of Alloy 1. A similar bright field micrograph is shown in Figure 8 from the last bead of Alloy 3. The conclusions drawn on the phases present are linked to diffraction experiments. Diffraction patterns were indexed by measuring the distance between the individual spots and the central spot on the film negatives. The lattice parameters for the individual phases are well know and corresponding distances for allowed reflections are well documented for given camera lengths [14 - 15]. Figure 9 shows a selected area (SA) electron diffraction pattern with a corresponding bright field image of the SA aperture. When the SA aperture is placed over the film (also seen in Figure 8) we see two {110} reflections of ferrite and reflections that suggest the presence of cementite, {100} and {200}. Additionally, the austenite spots {111} and {222} from the film are seen, but these disappear when the aperture is moved to either side of the film. Figure 10 shows a diffraction pattern taken from the grain to the left of the film where the {110} and {211} reflections of ferrite are seen. Again the {100} type spots are present that suggest the presence of cementite. Note the absence of the {111} type reflections that corresponds to austenite. Over the lath showing martensite in Figure 8,
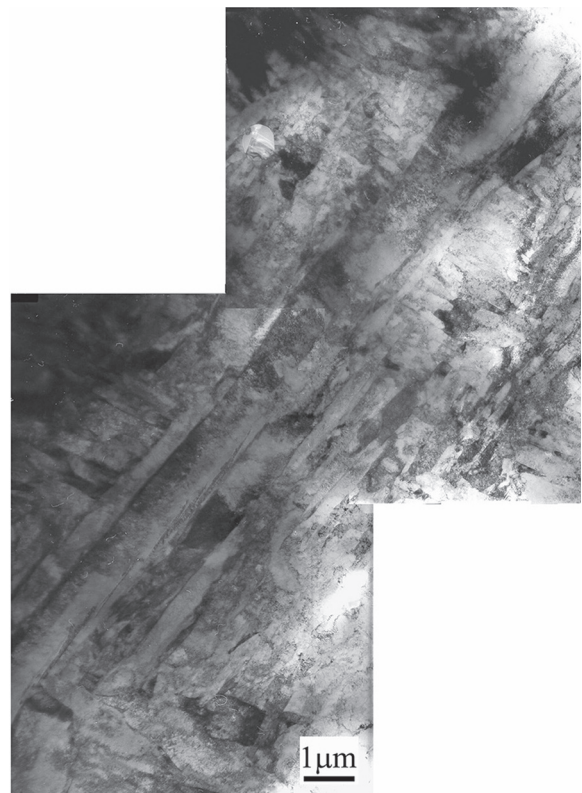

Figure 7. TEM micrograph from Alloy 1 showing a martensite / bainite microstructure.
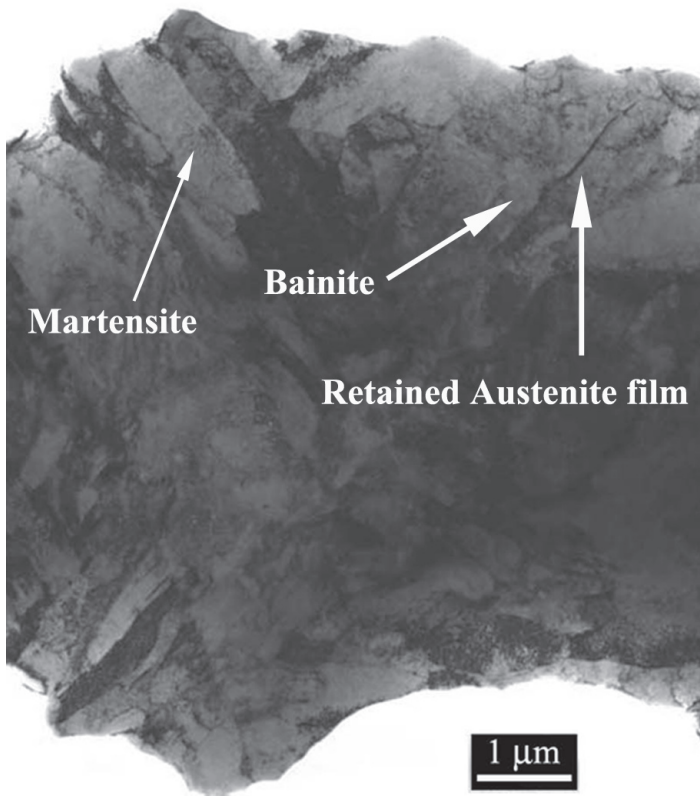
Figure 8. TEM micrograph from Alloy 3 showing martensite, bainite and austenite films in the microstructure.
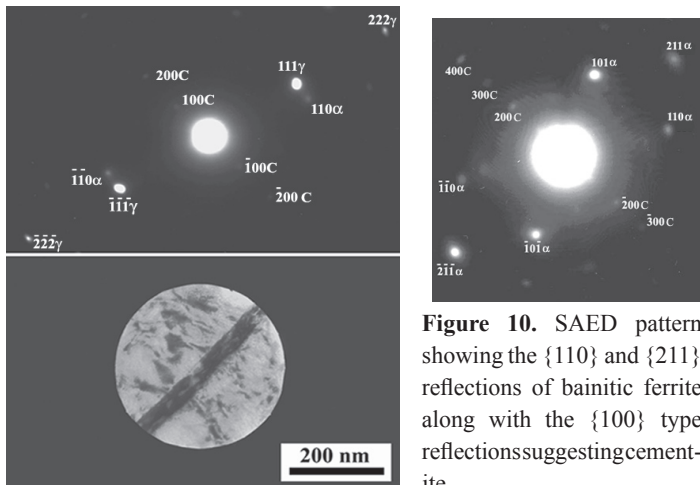

Figure 9. SAED pattern (above) corresponding to the bright field image of the SA aperture over the dark film (below). Results show the {111} and {222} spots from austenite, the {110} spots from ferrite and the {100} type spots suggesting cementite.

Figure 10. SAED pattern showing the {110} and {211} reflections of bainitic ferrite along with the {100} type reflections suggesting cementite.

no cementite or retained austenite reflections were found in diffraction patterns or dark field images which lead to suggestions of martensite. In Figure 8 it can be concluded that the microstructure is a mixture with bainite, martensite and films of retained austenite.

Finally APFIM was engaged primarily to investigate and accurately measure carbon behaviour on a local scale within the matrix, but also to monitor the manganese - nickel relationship. Different regions of the last bead were examined with the results of three runs from Alloy 1 and three runs from Alloy 3 presented in Table 4. The carbon level recorded in the first run of Alloy 1 is very low in comparison to the nominal composition while the second and third runs from Alloy 1 have a much higher level and are compatible to the nominal composition. Examining the results from Alloy 3, the carbon levels recorded for all runs are similar to the nominal composition. Ni and Mn is approximately at the nominal levels, except for run 2 of Alloy 3 where a significant depletion was seen.

Alloy	Ions	C	Mn	Ni
A 1	(34540)	0.007±0.002	1.89±0.07	7.06±0.29
A 1	(4286)	0.025±0.011	2.27±0.23	7.63±0.78
A 1	(4661)	0.055±0.016	2.54±0.23	7.63±0.81
A 3	(5034)	0.034±0.012	0.59±0.17	7.14±0.75
A 3	(72235)	0.022±0.003	0.46±0.02	5.98±0.18
A 3	(73389)	0.027±0.003	0.54±0.03	6.85±0.19

Table 4. The average levels of C, Mn and Ni in wt. % from individual APFIM runs. Also shown is the total No. of ions collected.

Discussion

The role of Mn and Ni in these weld alloys is very important. The alloying content of these elements and their effects after segregation are largely responsible for the individual phases present which in turn determine the mechanical properties.

It was seen that Alloys 1 and 2 had a higher hardness which was also maintained into the reheated beads. In comparison, Alloy 3 that had a lower hardness, softened further after reheating (Figure 3). Hardness results were reflected in both strength and toughness experiments. Alloys 1 and 2 had high strength and poor toughness while Alloy 3 had a somewhat lower strength and much better toughness. Taking all into consideration it was difficult to explain these properties and a greater understanding of the microstructure was needed.

Time-Temperature-Transformation (TTT) diagrams were calculated and presented in previous work that suggested a low carbon martensitic microstructure should form for Alloy 1 with all reasonable cooling rates. It was predicted that Alloy 3 would also form a martensitic microstructure although bainite could appear for very slow cooling. Calculations also predicted bainite formation for normal cooling rates if sufficient segregation took place [8].

With both SEM and SIMS, it was established firmly that significant segregation definitely takes place during solidification. In all three alloys as the weld metal first solidifies Mn and Ni are segregated into the molten weld metal. As a result, the Mn and Ni content is depleted at the dendrite centres and enriched in the inter-dendritic regions. It was established that Alloy 2 had the greatest segregation. Alloy 3, with the lowest nominal compositions (0.6 Mn and 6.6 Ni), recorded a difference of 0.38 wt. % and 1.72 wt. % between inter-dendritic regions and dendrite centres, for Mn and Ni respectively.

With a combination of TEM and APFIM it was found that the as-deposited microstructure was mixed and consisted of martensite, bainite and films of retained austenite. APFIM is consistant with the existance of

bainite and martensite in Alloy 1. The carbon level recorded in the first run was so low in comparison to the nominal composition it confirms the presence of bainite. The second and third runs from Alloy 1 had a much higher level of carbon that confirmed the presence of martensite. The results from Alloy 3 showed nominal carbon levels for all runs and confirmed the presence of martensite.

With a greater understanding of the microstructure the mechanical properties came into clearer perspective. Returning to the hardness measurements, they give a clear indication that Alloys 1 and 2 are predominantly martensitic. These conclusions are in line with the TTT diagrams presented in [8]. It is interesting to note that bainite also appears in the microstructure of Alloy 1 although the high Mn and Ni levels predicted to give a fully martensitic microstructure. From the hardness measurements it can be concluded that Alloy 3 is mainly bainitic. This does not fit perfectly with the calculated TTT diagrams, that predicted the formation of bainite only at long cooling times or with large amounts of segregation.

Taking the effect of reheating into consideration since toughness is measured in reheated weld metal, the hardness of Alloys 1 and 2 remains unchanged or decreases slightly with reheating. Alloy 3 softens further on reheating which would enhance toughness. The different effects of reheating give a clear indication of different amounts of martensite and bainite in the as-deposited microstructure. It may be concluded that the mechanical properties are critically dependent on how much martensite or bainite is present in the as-deposited microstructure and its response to reheating by subsequent beads. With high levels of Mn greater amounts of martensite form. In contrast, with lower levels of Mn greater amounts of bainite form.

Conclusions

Based on neural network simulations that showed Mn reductions in combination with Ni levels above 5 wt. % lead to large toughness increases while still maintaining strength, three experimental weld metals were produced using SMAW. Compositions of Mn levels at 0.6, 2.0 or 2.1 wt. % and Ni at 6.6, 7.2 and 9.2 wt. % respectively, were chosen to confirm the reliability of the model and to establish physically the weld metal characteristics.

Mechanical testing showed that Ni reductions with Mn levels at 2 wt. % lead to an increase in toughness. However the best Charpy toughness, 101 J at - 60 °C, was recorded with Mn at 0.6 wt. % and Ni at 6.6 wt. % as predicted by the model. A yield strength of 721 MPa was recorded with this composition. Hardness results showed that lower Mn and Ni levels lead to a softer weld metal.

Segregation of Ni and Mn to inter-dendritic regions was mapped using SIMS and quantified with EDX analysis. TEM investigations in conjunction with APFIM concluded a mixed microstructure of martensite, bainitie and retained austenite at an alloying level where a fully martensitic microstructure would normally be expected.

For higher levels of Mn a harder and more brittle mainly martensitic microstructure formed. At lower levels of Mn a softer, tougher and more easily tempered microstructure with greater amounts of bainite formed. Further microstructural studies are planned to investigate the tempering response of reheated regions for different Mn and Ni levels. These will further increase and develop correlations between the microstructure and mechanical properties.

References

1. L.-E. Svensson: Svetsaren, 54, January (1999).
2. D.J. Widgery, L. Karlsson, M. Muruganath & E. Keehan, Approaches to the development of high strength weld metals, 2nd Int. Symposium on High Strength Steel, Norway (2002).
3. M. Lord: Design and Modelling of Ultra - High Strength Steel Weld Deposits, Ph. D. Thesis, (1999), University of Cambridge: Cambridge.
4. Y. Kang, H.J. Kim, and S.K. Hwang: ISIJ International (Japan), 40 December (2000), p. 1237.
5. D.J.C. Mackay: Neural Computation. (1992), p. 448.
6. D.J.C. Mackay: Neural Computation. (1992), p. 415.
7. H.K.D.H. Bhadeshia: ISIJ International (Japan), 39, p. 966 October, (1999).
8. M. Muruganath, H. K. D. H. Bhadeshia, E. Keehan, H. O. Andrén, L. Karlsson, Strong and Tough Ferritic Steel Welds, Proc. 6th Int. Seminar, "Numerical Analysis of Weldability", Austria (2001)
9. M. K. Miller, A. Cerezo, M. G. Hetherington, G. D. W. Smith, Atom Probe Field Ion Microscopy, Clarendon Press, Oxford, 1996, p. 483.
10. H. O. Andrén, H. Norden, Scand. J. Metall. 8 (1979) 147.
11. H. O. Andrén, J. Phys. 47 (C7) (1986) 483.
12. U. Rolander, H. O. Andrén, J. Phys. 50 (C8) (1989) 529.
13. E. Keehan, L. Karlsson, M. Muruganath, H. O. Andrén, H. K. D. H. Bhadeshia, High Strength Steel Weld Metals - Developments with Ni and Mn, Proc. of the 7th Int. Welding Symposium, pp. 797-802, Kobe, Japan (2001).
14. K.W. Andrews, D. J. Dyson, S. R. Keown, Interpretation of Electron Diffraction Patterns, 2nd Ed., Adam Hilger Ltd., London (1971).
15. J. W. Edington, Practical Electron Microscopy in Material Science, The Macmillan Press Ltd., London (1975)